$NaLa(MoO_4)_2$ as a laser host material

S. B. Stevens and C. A. Morrison
Harry Diamond Laboratories, U. S. Army Laboratory Command, Adelphi, Maryland 20783

T. H. Allik
Science Applications International Corporation, 1710 Goodridge Drive, P. O. Box 1303, McLean, Virginia 22102

A. L. Rheingold and B. S. Haggerty
Department of Chemistry, University of Delaware, Newark, Delaware 19716
(Received 5 November 1990)

Crystallographic and optical properties of $NaLa(MoO_4)_2$ are presented. The positions of the Stark levels are reported for the $[LS]J$ manifolds of Nd^{3+} and Er^{3+} up to the absorption edge in this host material. A least-squares fit to the data was performed to obtain the crystal-field parameters. For Nd^{3+} the following crystal-field parameters were obtained: $B_{20}=519$, $B_{40}=-695$, $B_{44}=964$, $B_{60}=-190$, and $B_{64}=673+i384$ cm^{-1}, with a root-mean-square (rms) deviation of 7.7 cm^{-1}. For Er^{3+} we obtained $B_{20}=422$, $B_{40}=-507$, $B_{44}=839$, $B_{60}=-116$, and $B_{64}=409+i158$ cm^{-1}, with a rms deviation of 4.8 cm^{-1}. Intensity calculations based on fits to the experimental data yield line-to-line and multiplet branching ratios. The results of this investigation indicate that Er^{3+}:$NaLa(MoO_4)_2$ and Nd^{3+}:$NaLa(MoO_4)_2$ show promise as diode-pumped laser materials.

I. INTRODUCTION

The development of high-power laser-diode arrays and the successful use of these as pump sources for solid-state lasers have renewed interest in rare-earth spectroscopy. Rare-earths ions such as Nd^{3+}, Er^{3+} and Tm^{3+} have strong absorption transitions near 800 nm, where $Ga_{1-x}Al_xAs$ laser diodes emit peak powers in excess of 60 W per 1-cm bar. When lasers are pumped with these diodes, efficient output has been demonstrated for Nd^{3+} at 0.9, 1.0, and 1.3 μm[1-3], Er^{3+} at 1.6 and 2.9 μm, and Tm^{3+} at 1.9 μm.[4] Strong energy transfer from Er^{3+} or Tm^{3+} to Ho^{3+} has also produced lasing wavelengths near 2.1 μm. Current interests for new diode-pumped solid-state lasers are at eye-safe wavelengths near 1.5 μm, medical lasers at 1.9, 2.1, and 2.9 μm, and small single-frequency microchip lasers for injection seeding laser oscillators.[5,6]

$NaLa(MoO_4)_2$ (subsequently referred to as NLM) has been studied in the past for its suitability as a flashlamp-pumped laser host material.[7-9] Because of the relatively low-energy absorption edge around 370 nm (27,000 cm^{-1}), the thermal loading produced by a flashlamp made this material ill-suited for lasing applications. However, the results of this study and previous studies show promise for this host as a diode-pumped laser material. The rare-earth dopant (La^{3+}) site in NLM possesses attractive features. Its large size makes it suitable to be doped with rare-earth ions and Nd^{3+} can be fully substituted. The high dopant concentrations produce high absorption coefficients that lead to efficient absorption of light from a diode-laser pump, making this material well suited for the production of thin microchip lasers. The crystal field at the La^{3+} site has S_4 symmetry, and gives rise to smaller crystal-field splittings than the crystal field in D_2 garnet sites. For Er^{3+}, this weaker crystal field should yield a smaller probability for resonant up-conversion, which acts as a loss mechanism for eye-safe infrared lasers at 1.5 μm.[10]

The purpose of this paper is severalfold. First, detailed single-crystal x-ray measurements on NLM are presented. The lattice parameters have been previously reported,[11] but detailed measurements, including positions of the ions within the unit cell are not available in the literature. Second, we report the experimentally determined energy (Stark) levels for $Nd^{3+}(4f^3)$ and $Er^{3+}(4f^{11})$. Although some spectroscopic properties have been reported earlier for Nd^{3+}, they are for only the low-lying levels, and a discrepancy in the assignments has been seen.[7,9] Third, theoretical intensity calculations were performed on the experimental energy-level data for Nd^{3+} and Er^{3+}. Using the crystal-field components, A_{kq}, the branching ratios for line-to-line transitions are predicted for Nd^{3+} and Er^{3+}.

II. CRYSTAL GROWTH AND STRUCTURE

The NLM crystals used in this study were grown from oriented seeds in the early 1970's at the National Bureau of Standards. The crystals were approximately 1.0 cm in diameter and 2.0 cm long with an optical quality inferior to laser samples such as YAG and YLF. The Nd doping concentrations of six growth runs were 0.1, 1, 5, 10, 20, and 100 at. % substitution for La. Two boules of 2 and 0.5 at. % Er were also grown. The optical data presented here are for the 0.1 at. % Nd doping and the 2 at. % Er doping. The x-ray data were obtained with the 0.1 at. % Nd-doped crystal.

The crystal structure analysis was performed at 23(1) °C, on an automated Nicolet $R3m/\mu m$ diffractometer

TABLE I. Summary of crystallographic data for NaLa(MoO$_4$)$_2$.

(a) Crystal parameters			
Formula	NaLa(MoO$_4$)$_2$	Cryst. dimensions	0.2×0.2×0.3 mm^3
Space group	$I4_1a$ (No. 88)	Crystal color	colorless
Crystal system	tetragonal	D, calculated	4.772 g/cm^3
a	5.3433(11) Å	μ (Mo $K\alpha$)	100.24 cm^{-1}
c	11.7432(19) Å	Temperature	23(1) °C
V	335.27(12) Å^3	T(max)/T(min)	0.042/0.003=14
Z	4		

(b) Data Collection			
Diffractometer	Nicolet $R3m/\mu$	Rflns. collected	451
Monochromator	graphite	independent rflns.	406
Scan technique	Wyckoff	R (merg)	4.61%
Radiation	Mo $K\alpha$ (λ=0.71073 Å)	Independant rflns.	143
2θ scan range	4−70°	Std. rflns.	3 std/97 rflns
Data collected (h,k,l)	9,9,19	Var. in stds.	<1%
Scan speed	var. 5-20 deg/min		

(c) Refinement			
$R(F)$	8.51%	$\Delta(\rho)$	2.481 e Å^{-3}
$R(wF)$	9.24%	N_0/N_v	9.53
Δ/σ(max)	0.002	Goodness of fit	1.75

with an incident beam graphite monochromator and Mo $K\alpha$ radiation (λ=0.71073 Å). The unit cell was obtained from the least-squares refinement of 25 reflections ($20° < \theta < 25°$) yielding the lattice parameters a=5.3433(11) Å, c=11.7432(19) Å, and V=335.27(12) Å^3. Systematic absences in the diffraction data (hkl, $k+l=2n+1$; $hk0, h,k=2n+1$; $0kl, k+l=2n+1$; $hhl, l=2n+1$; $00l, l=4n+1$; and $0k0, k=2n+1$) uniquely established the space group as tetragonal $I4_1a$ with Z=4. The structure is isomorphous with those of the minerals scheelite (CaWO$_4$) and wulfenite (PbMoO$_4$).[12] Intensity data were collected using Wyckoff scans (4° to 70°), with a variable scan rate of 5 to 20 deg/min. Three standard reflections monitored every 97 reflections showed insignificant variation (<1%). The 143 independent, observed [$F_0 > 5\sigma(F_0)$] data were used to refine the structure to R_F=8.51% and R_{wF}=9.24%. These somewhat high R factors reflect the inherent disorder in the average unit cell due to the variable presence of Na or La, which occupy the same site. Na and La were each refined at half occupancy to account for the stoichiometry of the Scheelite structure formula. All atoms were refined with anisotropic thermal parameters. All computer programs and the sources of the scattering factors are contained in the SHELXTL program library.[13]

TABLE II. Fractional atomic coordinates.

Ion	Position	x [a]	y [a]	z [a]
LaNa	4(b)	0	0	0.5
Mo	4(a)	0	0	0
O	16(f)	0.2319	0.1386	0.0746

[a]Expressed as fractions of the lattice parameters.

Table I summarizes the crystallographic data. The positions of the ions in the unit cell are given in Table II. These positions correspond to setting 1 for space group $I4_1a-C_{4h}^6$ (No. 88) in the International Tables for X-ray Crystallography.[14] Figure 1 shows the molecular structure and labeling scheme used for the unit cell.

III. SPECTRAL ANALYSIS

The determination of individual Stark levels of the Nd^{3+} and Er^{3+} ions were determined by recording spectra at 17±3 K with a Perkin-Elmer Lambda 9 spectrophotometer. Fluorescence spectra were also recorded with a Spex F222 or a Tracor Northern TN-6600 spectrometer. The $^4F_{3/2}$ to $^4I_{11/2}$ fluorescence spectra of Nd^{3+}:NLM and Nd^{3+}:YAG are shown together in Fig. 2 to illustrate the qualitative differences in the spectra. Detailed experimental procedures have been given before and will not be duplicated here.[15,16] Tables III and IV list the experimentally determined energy levels for Nd^{3+} and Er^{3+}, respectively.

The free-ion wave functions were calculated by diagonalizing, in a Russell-Saunders basis of [LS]J states, a Hamiltonian containing the Coulomb, spin orbit, L^2, $G(G_2)$, and $G(R_7)$ interactions.[17] The free-ion parameters chosen were those obtained by Carnall, Fields, and

TABLE III. Energy levels of Nd^{3+} in $NaLa(MoO_4)_2$.

$^{2S+1}L_J$ centroids (cm^{-1})	Level number	Γ_n[a]	Energy (cm^{-1}) Theor.	Expt.	Free-ion mixture (%)		
$^4I_{9/2}$	1	7,8	−3	0	$99.64\,^4I_{9/2}$	$+0.24\,^4I_{11/2}$	$+0.06\,^4I_{13/2}$
(198)	2	7,8	100	92	$98.79\,^4I_{9/2}$	$+1.13\,^4I_{11/2}$	$+0.03\,^4F_{3/2}$
	3	5,6	157	160	$99.48\,^4I_{9/2}$	$+0.41\,^4I_{11/2}$	$+0.08\,^4I_{13/2}$
	4	5,6	246	235	$98.89\,^4I_{9/2}$	$+1.04\,^4I_{11/2}$	$+0.04\,^4I_{13/2}$
	5	7,8	399	412	$99.70\,^4I_{9/2}$	$+0.24\,^4I_{11/2}$	$+0.05\,^4I_{13/2}$
$^4I_{11/2}$	6	7,8	1957	1960	$99.19\,^4I_{11/2}$	$+0.43\,^4I_{13/2}$	$+0.28\,^4I_{9/2}$
(2060)	7	5,6	1996	1999	$98.71\,^4I_{11/2}$	$+0.63\,^4I_{9/2}$	$+0.61\,^4I_{13/2}$
	8	7,8	2007	2013	$99.03\,^4I_{11/2}$	$+0.51\,^4I_{13/2}$	$+0.35\,^4I_{9/2}$
	9	5,6	2046		$98.62\,^4I_{11/2}$	$+0.90\,^4I_{13/2}$	$+0.41\,^4I_{9/2}$
	10	5,6	2146		$99.20\,^4I_{11/2}$	$+0.40\,^4I_{9/2}$	$+0.38\,^4I_{13/2}$
	11	7,8	2172	2160	$98.80\,^4I_{11/2}$	$+1.00\,^4I_{9/2}$	$+0.14\,^4I_{13/2}$
$^4I_{13/2}$	12	5,6	3919	3916	$99.25\,^4I_{13/2}$	$+0.37\,^4I_{15/2}$	$+0.30\,^4I_{11/2}$
(4044)	13	7,8	3952	3946	$99.15\,^4I_{13/2}$	$+0.42\,^4I_{15/2}$	$+0.36\,^4I_{11/2}$
	14	5,6	3968	3967	$98.82\,^4I_{13/2}$	$+0.62\,^4I_{15/2}$	$+0.44\,^4I_{11/2}$
	15	7,8	4008	4009	$98.83\,^4I_{13/2}$	$+0.89\,^4I_{15/2}$	$+0.20\,^4I_{11/2}$
	16	5,6	4115	4120	$98.91\,^4I_{13/2}$	$+0.73\,^4I_{11/2}$	$+0.31\,^4I_{15/2}$
	17	7,8	4158		$99.17\,^4I_{13/2}$	$+0.52\,^4I_{11/2}$	$+0.22\,^4I_{15/2}$
	18	5,6	4161	4166	$99.26\,^4I_{13/2}$	$+0.41\,^4I_{11/2}$	$+0.28\,^4I_{15/2}$
$^4I_{15/2}$	19	5,6	5843	5849	$99.49\,^4I_{15/2}$	$+0.39\,^4I_{13/2}$	$+0.04\,^4F_{7/2}$
(6084)	20	5,6	5903	5900	$99.49\,^4I_{15/2}$	$+0.38\,^4I_{13/2}$	$+0.06\,^4F_{9/2}$
	21	7,8	5949	5944	$99.59\,^4I_{15/2}$	$+0.31\,^4I_{13/2}$	$+0.05\,^4I_{11/2}$
	22	7,8	6011	6012	$99.54\,^4I_{15/2}$	$+0.37\,^4I_{13/2}$	$+0.03\,^4I_{11/2}$
	23	7,8	6201		$99.55\,^4I_{15/2}$	$+0.37\,^4I_{13/2}$	$+0.05\,^4I_{11/2}$
	24	5,6	6220	6211	$99.51\,^4I_{15/2}$	$+0.42\,^4I_{13/2}$	$+0.02\,^4I_{11/2}$
	25	7,8	6276		$99.47\,^4I_{15/2}$	$+0.47\,^4I_{13/2}$	$+0.03\,^4I_{11/2}$
	26	5,6	6304	6313	$99.55\,^4I_{15/2}$	$+0.38\,^4I_{13/2}$	$+0.04\,^4F_{7/2}$
$^4F_{3/2}$	27	7,8	11401	11393	$99.34\,^4F_{3/2}$	$+0.21\,^2H_{9/2}$	$+0.19\,^4F_{7/2}$
(11444)	28	5,6	11464	11472	$98.24\,^4F_{3/2}$	$+1.28\,^4F_{5/2}$	$+0.21\,^4F_{7/2}$
$^4F_{5/2}$	29	7,8	12406	12418	$92.38\,^4F_{5/2}$	$+6.62\,^2H_{9/2}$	$+0.56\,^4F_{7/2}$
(12475)	30	5,6	12454	12456	$85.43\,^4F_{5/2}$	$+12.17\,^2H_{9/2}$	$+1.41\,^4F_{3/2}$
	31	5,6	12523	12508	$93.77\,^4F_{5/2}$	$+5.26\,^2H_{9/2}$	$+0.69\,^4F_{7/2}$

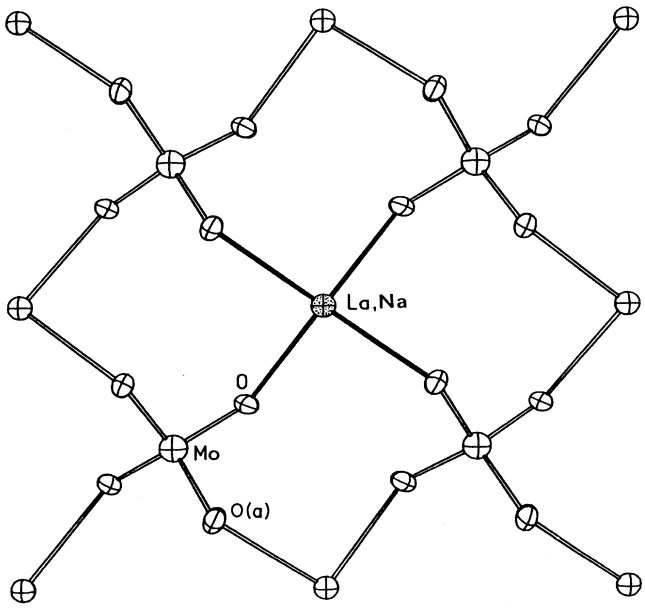

FIG. 1. Molecular structure of $NaLa(MoO_4)_2$. Ellipsoids are at 35% probability.

Rajnak[18] for the triply ionized lanthanide ions in aqueous solution. Using their set of free-ion parameters, we calculated reduced matrix elements of U_2, U_4, and U_6 between all of the intermediate-coupled wave functions representing the multiplets of the electronic configuration $4f^N$ of the free ion.

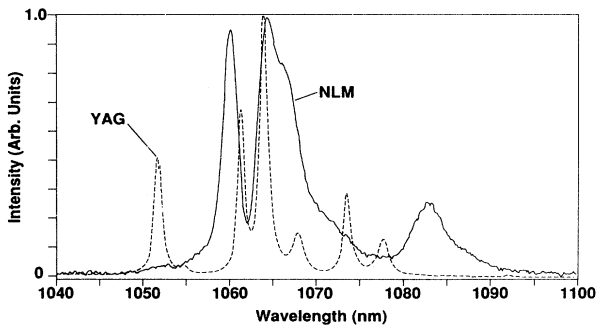

FIG. 2. Unpolarized fluorescence spectra of the $^4F_{3/2}$ to $^4I_{11/2}$ transitions in Nd^{3+}:$NaLa(MoO_4)_2$ and Nd^{3+}:YAG at room temperature.

TABLE III. (*Continued.*)

$^{2S+1}L_J$ centroids (cm^{-1})	Level number	Γ_n[a]	Energy (cm^{-1}) Theor.	Expt.	Free-ion mixture (%)		
$^2H_{9/2}$	32	7,8	12 526	12 528	99.08 $^2H_{9/2}$	+0.78 $^4F_{5/2}$	+0.05 $^4F_{7/2}$
(12614)	33	5,6	12 543	12 556	84.04 $^2H_{9/2}$	+15.50 $^4F_{5/2}$	+0.26 $^4F_{7/2}$
	34	5,6	12 638	12 625	97.72 $^2H_{9/2}$	+2.11 $^4F_{5/2}$	+0.06 $^4F_{7/2}$
	35	7,8	12 657	12 674	96.75 $^2H_{9/2}$	+2.58 $^4F_{5/2}$	+0.33 $^4F_{7/2}$
	36	7,8	12 728	12 711	96.53 $^2H_{9/2}$	+3.21 $^4F_{5/2}$	+0.06 $^4F_{7/2}$
$^4F_{7/2}$	37	7,8	13 365	13 364	98.54 $^4F_{7/2}$	+0.58 $^4F_{9/2}$	+0.38 $^2H_{9/2}$
(13439)	38	5,6	13 402	13 403	96.33 $^4F_{7/2}$	+1.36 $^4F_{5/2}$	+1.27 $^4S_{3/2}$
$^4S_{3/2}$	39	7,8	13 484	13 484	96.14 $^4S_{3/2}$	+3.49 $^4F_{7/2}$	+0.11 $^2H_{9/2}$
(13489)	40	5,6	13 487		83.09 $^4S_{3/2}$	+16.41 $^4F_{7/2}$	+0.20 $^4G_{5/2}$
	41	5,6	13 493		84.04 $^4F_{7/2}$	+15.23 $^4S_{3/2}$	+0.40 $^4F_{9/2}$
	42	7,8	13 517	13 517	95.64 $^4F_{7/2}$	+3.35 $^4S_{3/2}$	+0.52 $^4F_{5/2}$
$^4F_{9/2}$	43	5,6	14 633	14 624	99.31 $^4F_{9/2}$	+0.32 $^4F_{7/2}$	+0.09 $^2G_{7/2}$
(14712)	44	7,8	14 658	14 658	99.25 $^4F_{9/2}$	+0.43 $^4F_{7/2}$	+0.11 $^4F_{5/2}$
	45	7,8	14 745	14 736	99.08 $^4F_{9/2}$	+0.32 $^4F_{7/2}$	+0.25 $^2H_{11/2}$
	46	5,6	14 746	14 758	99.10 $^4F_{9/2}$	+0.37 $^4F_{7/2}$	+0.31 $^2H_{11/2}$
	47	7,8	14 810	14 815	99.57 $^4F_{9/2}$	+0.20 $^2G_{7/2}$	+0.08 $^2H_{11/2}$
$^2H_{11/2}$	48	5,6	15 912		99.53 $^2H_{11/2}$	+0.34 $^2G_{7/2}$	+0.07 $^4F_{7/2}$
(15939)	49	7,8	15 914		99.42 $^2H_{11/2}$	+0.33 $^2G_{7/2}$	+0.11 $^4F_{9/2}$
	50	7,8	15 937		99.44 $^2H_{11/2}$	+0.37 $^2G_{7/2}$	+0.14 $^4F_{9/2}$
	51	5,6	15 944	15 944	99.58 $^2H_{11/2}$	+0.17 $^4F_{9/2}$	+0.14 $^2G_{7/2}$
	52	7,8	15 955		99.55 $^2H_{11/2}$	+0.20 $^2G_{7/2}$	+0.11 $^4F_{9/2}$
	53	5,6	15 981		99.29 $^2H_{11/2}$	+0.32 $^2G_{7/2}$	+0.19 $^4F_{9/2}$
$^4G_{5/2}$	54	5,6	16 989	16 984	83.39 $^4G_{5/2}$	+16.31 $^2G_{7/2}$	+0.10 $^4F_{7/2}$
(17098)	55	7,8	17 040	17 050	88.52 $^4G_{5/2}$	+10.94 $^2G_{7/2}$	+0.18 $^4F_{9/2}$
	56	5,6	17 112	17 103	58.01 $^4G_{5/2}$	+41.35 $^2G_{7/2}$	+0.26 $^2H_{11/2}$
$^2G_{7/2}$	57	7,8	17 211		98.18 $^2G_{7/2}$	+1.07 $^4G_{5/2}$	+0.42 $^2H_{11/2}$
(17212)	58	5,6	17 224	17 226	95.56 $^2G_{7/2}$	+3.90 $^4G_{5/2}$	+0.39 $^2H_{11/2}$
	59	7,8	17 284	17 286	89.29 $^2G_{7/2}$	+9.97 $^4G_{5/2}$	+0.40 $^2H_{11/2}$
	60	5,6	17 395	17 394	53.99 $^4G_{5/2}$	+45.63 $^2G_{7/2}$	+0.13 $^2H_{11/2}$

[a]Irreducible representation, Γ_n, of the S_4 group.

A separate program then selected the reduced matrix elements between the free-ion multiplets in a truncated basis (13 multiplets for Nd^{3+} and 15 multiplets for Er^{3+}), set up the crystal spaces for the given crystal-field symmetry (S_4 for NLM), and diagonalized the crystal-field Hamiltonian in that space of multiplets. The procedure is discussed in more detail by Morrison and Leavitt.[19]

The experimentally determined Stark level positions of the rare-earth dopant ion are fit assuming a crystal field of the form:

$$H_{\mathrm{CEF}} = \sum_{i,k,q} B_{kq}^{*} C_{kq}(\hat{\mathbf{r}}_i) , \quad (k=2,4,6; q=0,4; 1 \le i \le N) , \tag{1}$$

where the B_{kq} are the crystal-field parameters, and the $C_{kq}(\hat{\mathbf{r}}_i)$ are tensor operators related to the spherical harmonics by

$$C_{kq}(\hat{\mathbf{r}}_i) = \left[\frac{4\pi}{2k+1} \right]^{1/2} Y_{kq}(\theta_i, \phi_i) . \tag{2}$$

In S_4 symmetry, which is the site symmetry of both Na and La, the crystal-field parameters are B_{20}, B_{40}, B_{44}, B_{60}, and B_{64}. With no loss of generality, B_{44} can be chosen to be real and positive, fixing the rotational degree of freedom associated with the tensor quantities.[20] With this choice, B_{64} is in general complex. The crystal-field parameters B_{kq} are then determined by minimizing the squared difference of the calculated and experimental energies. The centroids of each $[LS]J$ multiplet are allowed to vary freely during the fitting and are considered experimental data in the final analysis.

Data for Nd^{3+} in NLM have been previously reported[9] and fit by Onopko.[21] Because he chose all crystal-field parameters to be real (essentially D_{2d} symmetry), comparisons of the energy levels calculated using his parameters with the experimental data were rather poor. Consequently, the starting values of B_{kq} for both Nd^{3+} and Er^{3+} were from $CaWO_4$.[22]

The calculation for Nd^{3+} included 47 experimental levels and 60 theoretical levels and gave a rms deviation of 7.7 cm^{-1}. We obtained the following crystal-field parameters for Nd^{3+}: $B_{20}=519$, $B_{40}=-695$, $B_{44}=964$, $B_{60}=-190$, and $B_{64}=673+i384$ cm^{-1}. The calculation for Er^{3+} included 52 experimental levels and 76 theoretical levels and gave a rms deviation of 4.8 cm^{-1}. We obtained the following crystal-field parameters for Er^{3+}:

TABLE IV. Energy levels of Er^{3+} in $NaLa(MoO_4)_2$.

$^{2S+1}L_J$ centroids (cm^{-1})	Level number	Γ_n[a]	Energy (cm^{-1}) Theor.	Expt.	Free-ion mixture (%)		
$^4I_{15/2}$	1	5,6	0	0	$99.98\,^4I_{15/2}$	$+0.01\,^4I_{13/2}$	
(136)	2	7,8	9	18	$99.99\,^4I_{15/2}$	$+0.01\,^4I_{13/2}$	
	3	5,6	40	32	$99.97\,^4I_{15/2}$	$+0.02\,^4I_{13/2}$	
	4	7,8	57	57	$99.97\,^4I_{15/2}$	$+0.03\,^4I_{13/2}$	
	5	7,8	192	184	$99.97\,^4I_{15/2}$	$+0.02\,^4I_{13/2}$	$+0.01\,^4F_{9/2}$
	6	7,8	227	227	$99.97\,^4I_{15/2}$	$+0.01\,^4I_{13/2}$	$+0.01\,^2H_{11/2}$
	7	5,6	255	255	$99.96\,^4I_{15/2}$	$+0.01\,^4I_{13/2}$	$+0.01\,^4F_{9/2}$
	8	5,6	283	291	$99.96\,^4I_{15/2}$	$+0.01\,^4I_{13/2}$	$+0.01\,^4F_{9/2}$
$^4I_{13/2}$	9	7,8	6 521	6 519	$99.92\,^4I_{13/2}$	$+0.06\,^4I_{11/2}$	$+0.01^4I_{9/2}$
(6615)	10	5,6	6 523	6 528	$99.94\,^4I_{13/2}$	$+0.04\,^4I_{11/2}$	$+0.01\,^4I_{15/2}$
	11	5,6	6 573	6 571	$99.87\,^4I_{13/2}$	$+0.10\,^4I_{11/2}$	$+0.01^4I_{15/2}$
	12	7,8	6 628	6 626	$99.91\,^4I_{13/2}$	$+0.04\,^4I_{15/2}$	$+0.03\,^4I_{11/2}$
	13	5,6	6 660	6 660	$99.90\,^4I_{13/2}$	$+0.05\,^4I_{11/2}$	$+0.03\,^4I_{15/2}$
	14	7,8	6 677	6 676	$99.89\,^4I_{13/2}$	$+0.05\,^4I_{11/2}$	$+0.02\,^4I_{9/2}$
	15	5,6	6 696	6 698	$99.93\,^4I_{13/2}$	$+0.03\,^4I_{11/2}$	$+0.01\,^4I_{15/2}$
$^4I_{11/2}$	16	7,8	10 181	10 175	$99.86\,^4I_{11/2}$	$+0.06\,^4I_{9/2}$	$+0.04\,^4F_{9/2}$
(10234)	17	5,6	10 191	10 192	$99.91\,^4I_{11/2}$	$+0.05\,^4I_{13/2}$	$+0.01\,^4I_{9/2}$
	18	5,6	10 234	10 235	$99.83\,^4I_{11/2}$	$+0.10\,^4I_{13/2}$	$+0.04\,^4I_{9/2}$
	19	7,8	10 251	10 253	$99.85\,^4I_{11/2}$	$+0.07\,^4I_{13/2}$	$+0.03\,^4I_{9/2}$
	20	5,6	10 265		$99.84\,^4I_{11/2}$	$+0.07\,^4I_{13/2}$	$+0.04\,^4F_{9/2}$
	21	7,8	10 272	10 273	$99.87\,^4I_{11/2}$	$+0.04\,^4I_{13/2}$	$+0.03\,^4I_{9/2}$
$^4I_{9/2}$	22	7,8	12 360	12 366	$99.93\,^4I_{9/2}$	$+0.02\,^4F_{9/2}$	$+0.02\,^4I_{13/2}$
(12483)	23	5,6	12 454		$99.89\,^4I_{9/2}$	$+0.06\,^4I_{11/2}$	$+0.01\,^2H_{11/2}$
	24	5,6	12 497	12 497	$99.92\,^4I_{9/2}$	$+0.04\,^4I_{11/2}$	$+0.01\,^2H_{11/2}$
	25	7,8	12 503		$99.81\,^4I_{9/2}$	$+0.06\,^4I_{11/2}$	$+0.04\,^4S_{3/2}$
	26	7,8	12 592	12 585	$99.89\,^4I_{9/2}$	$+0.04\,^4I_{11/2}$	$+0.03\,^4F_{9/2}$
$^4F_{9/2}$	27	7,8	15 230	15 228	$99.89\,^4F_{9/2}$	$+0.03\,^4I_{11/2}$	$+0.03\,^4I_{9/2}$
(15295)	28	5,6	15 263	15 260	$99.88\,^4F_{9/2}$	$+0.04\,^2H_{11/2}$	$+0.02\,^4I_{11/2}$
	29	7,8	15 267	15 274	$99.88\,^4F_{9/2}$	$+0.03\,^2H_{11/2}$	$+0.02\,^4I_{11/2}$
	30	7,8	15 335	15 333	$99.88\,^4F_{9/2}$	$+0.04\,^4F_{5/2}$	$+0.03\,^4I_{11/2}$
	31	5,6	15 380	15 380	$99.92\,^4F_{9/2}$	$+0.04\,^4I_{11/2}$	$+0.01\,^4I_{15/2}$
$^4S_{3/2}$	32	5,6	18 355	18 352	$97.46\,^4S_{3/2}$	$+2.49\,^4H_{11/2}$	$+0.01\,^4G_{11/2}$
(18402)	33	7,8	18 417	18 420	$98.78\,^4S_{3/2}$	$+1.11\,^2H_{11/2}$	$+0.04\,^4I_{9/2}$
$^2H_{11/2}$	34	5,6	19 087	19 091	$99.56\,^2H_{11/2}$	$+0.24\,^4F_{7/2}$	$+0.04\,^4F_{9/2}$
(19155)	35	7,8	19 110		$99.83\,^2H_{11/2}$	$+0.04\,^4F_{7/2}$	$+0.03\,^4F_{9/2}$
	36	7,8	19 148	19 139	$99.64\,^2H_{11/2}$	$+0.26\,^4S_{3/2}$	$+0.02\,^4F_{7/2}$
	37	5,6	19 189	19 183	$97.78\,^2H_{11/2}$	$+1.92\,^4S_{3/2}$	$+0.22\,^4F_{7/2}$
	38	7,8	19 198	19 198	$98.89\,^2H_{11/2}$	$+0.84\,^4S_{3/2}$	$+0.21\,^4F_{7/2}$
	39	5,6	19 208	19 220	$99.28\,^2H_{11/2}$	$+0.53\,^4S_{3/2}$	$+0.09\,^4F_{7/2}$

$B_{20}=422$, $B_{40}=-507$, $B_{44}=839$, $B_{60}=-116$, and $B_{64}=409+i158$ cm^{-1}. The results of this fitting procedure are given in Table III for Nd^{3+}:NLM and in Table IV for Er^{3+}:NLM. It was not possible to measure peaks for Er^{3+} past the 59th level because of the absorption edge of $NaLa(MoO_4)_2$ at around 370 nm.

Because NLM is a partially disordered host, in that the cation site is randomly occupied by Na or La ions, the linewidths are correspondingly broadened and the reported energy levels are only good to within 5 cm^{-1}. Thus, rms deviations lower than those already obtained would not be significant

We assume that the crystal-field parameter B_{kq} can be factored into a host-dependent crystal-field component A_{kq} and an ion-dependent quantity ρ_k:

$$B_{kq}=\rho_k A_{kq} . \quad (3)$$

Values of ρ_k for each of the ions in the lanthanide series are given elsewhere.[19] Using Eq. (3), we calculated experimental values for the evenfold A_{kq} from the tabulated ρ_k and experimental best-fit B_{kq} for both the Er^{3+}:NLM and Nd^{3+}:NLM data sets. We averaged the resulting A_{kq} and the average values were used to compute B_{kq}'s for the entire lanthanide series, given in Table V.

Theoretical values for A_{kq} (denoted by A_{kq}^{theor}) are obtained from x-ray data by calculating lattice sums centered around the La (Na) site in the crystal structure. The effective charge on the La (Na) site, q_{La} was taken as $+2$ in units of the electron charge. The molybdenum charge, q_{Mo} and oxygen charge, q_{O}, were chosen such

TABLE IV. (*Continued.*)

$^{2S+1}L_J$ centroids (cm^{-1})	Level number	Γ_n[a]	Energy (cm^{-1}) Theor.	Expt.	Free-ion mixture (%)		
$^4F_{7/2}$	40	7,8	20 466	20 471	99.58 $^4H_{7/2}$	+0.13 $^4F_{5/2}$	+0.13 $^2H_{11/2}$
(20522)	41	5,6	20 488	20 488	99.52 $^4F_{7/2}$	+0.39 $^2H_{11/2}$	+0.02 $^4F_{5/2}$
	42	5,6	20 559	20 555	99.44 $^4H_{7/2}$	+0.26 $^4F_{5/2}$	+0.17 $^2H_{11/2}$
	43	7,8	20 578	20 576	99.72 $^4F_{7/2}$	+0.16 $^2H_{11/2}$	+0.03 $^4G_{11/2}$
$^4F_{5/2}$	44	5,6	22 152	22 153	98.15 $^4F_{5/2}$	+1.50 $^4F_{3/2}$	+0.23 $^4F_{7/2}$
(22175)	45	5,6	22 167	22 168	95.12 $^4F_{5/2}$	+4.71 $^4F_{3/2}$	+0.07 $^2H_{11/2}$
	46	7,8	22 199	22 198	99.62 $^4F_{5/2}$	+0.13 $^4F_{7/2}$	+0.07 $^4F_{3/2}$
$^4F_{3/2}$	47	5,6	22 501		93.65 $^4F_{3/2}$	+6.18 $^4F_{5/2}$	+0.11 $^4F_{7/2}$
(22513)	48	7,8	22 548	22 548	99.64 $^4F_{3/2}$	+0.11 $^4F_{7/2}$	+0.07 $^4F_{5/2}$
$^2G_{9/2}$	49	7,8	24 455		99.83 $^2G_{9/2}$	+0.10 $^4G_{11/2}$	+0.02 $^2K_{15/2}$
(24564)	50	5,6	24 542	24 540	99.54 $^2G_{9/2}$	+0.22 $^4G_{11/2}$	+0.19 $^2K_{15/2}$
	51	7,8	24 567	24 570	99.46 $^2G_{9/2}$	+0.27 $^4G_{11/2}$	+0.21 $^2K_{15/2}$
	52	5,6	24 575		99.54 $^2G_{9/2}$	+0.22 $^4G_{11/2}$	+0.18 $^2K_{15/2}$
	53	7,8	24 650	24 649	99.68 $^2G_{9/2}$	+0.20 $^2K_{15/2}$	+0.04 $^4F_{5/2}$
$^4G_{11/2}$	54	5,6	26 288	26 288	98.80 $^4G_{11/2}$	+0.70 $^4G_{9/2}$	+0.30 $^2G_{9/2}$
(26377)	55	7,8	26 295		99.15 $^4G_{11/2}$	+0.30 $^4G_{9/2}$	+0.23 $^2G_{9/2}$
	56	7,8	26 342	26 338	99.03 $^4G_{11/2}$	+0.70 $^4G_{9/2}$	+0.13 $^2G_{9/2}$
	57	5,6	26 404	26 392	99.62 $^4G_{11/2}$	+0.12 $^2G_{9/2}$	+0.08 $^2G_{7/2}$
	58	7,8	26 456	26 462	99.24 $^4G_{11/2}$	+0.60 $^2K_{15/2}$	+0.06 $^4G_{9/2}$
	59	5,6	26 465	26 476	99.56 $^4G_{11/2}$	+0.20 $^2K_{15/2}$	+0.15 $^4G_{9/2}$
$^4G_{9/2}$	60	5,6	27 438		94.46 $^4G_{9/2}$	+3.98 $^2G_{7/2}$	+1.29 $^2K_{15/2}$
(27 478)	61	7,8	27 444		95.44 $^4G_{9/2}$	+2.83 $^2G_{7/2}$	+1.47 $^2K_{15/2}$
	62	7,8	27 487		97.65 $^4G_{9/2}$	+1.54 $^2K_{15/2}$	+0.49 $^4G_{11/2}$
	63	5,6	27 503		97.76 $^4G_{9/2}$	+0.85 $^2K_{15/2}$	+0.72 $^4G_{11/2}$
	64	7,8	27 515		98.14 $^4G_{9/2}$	+1.24 $^2K_{15/2}$	+0.42 $^4G_{11/2}$
$^2K_{15/2}$	65	5,6	27 551		97.17 $^2K_{15/2}$	+1.44 $^4G_{9/2}$	+1.24 $^2G_{7/2}$
(27 800)	66	7,8	27 552		95.40 $^2K_{15/2}$	+3.23 $^4G_{9/2}$	+1.19 $^2G_{7/2}$
	67	5,6	27 808		96.85 $^2K_{15/2}$	+3.00 $^2G_{7/2}$	+0.08 $^4G_{9/2}$
	68	7,8	27 818		92.10 $^2K_{15/2}$	+7.56 $^2G_{7/2}$	+0.18 $^4G_{9/2}$
	69	7,8	27 855		76.92 $^2K_{15/2}$	+22.62 $^2G_{7/2}$	+0.22 $^4G_{9/2}$
	70	5,6	27 909		81.39 $^2K_{15/2}$	+17.64 $^2G_{7/2}$	+0.77 $^4G_{9/2}$
	71	7,8	27 931		97.43 $^2K_{15/2}$	+1.89 $^2G_{7/2}$	+0.56 $^4G_{11/2}$
	72	5,6	27 937		91.64 $^2K_{15/2}$	+7.91 $^2G_{7/2}$	+0.21 $^4G_{9/2}$
$^2G_{7/2}$	73	7,8	28 007		89.51 $^2G_{7/2}$	+8.74 $^2K_{15/2}$	+1.57 $^4G_{9/2}$
(27 981)	74	5,6	28 017		81.29 $^2G_{7/2}$	+15.86 $^2K_{15/2}$	+2.72 $^4G_{9/2}$
	75	5,6	28 031		84.10 $^2G_{7/2}$	+14.18 $^2K_{15/2}$	+1.51 $^4G_{9/2}$
	76	7,8	28 037		73.85 $^2G_{7/2}$	+23.79 $^2K_{15/2}$	+2.18 $^4G_{9/2}$

[a]Irreducible representation, Γ_n, of the S_4 group.

that the overall charge on the (MoO_4) is -2, giving $q_{Mo}=-2-4q_O$. The values for A_{kq}^{theor} are then obtained as a result of the lattice sum and are given by

$$A_{kq}^{theor}=a_{kq}+q_O b_{kq} \ . \tag{4}$$

The optimum value for the oxygen charge q_O is found by minimizing the variance, $\sum_{k,q}[A_{kq}^{theor}(q_O)-A_{kq}^{expt}]^2$, with respect to q_O. The value of the oxygen charge determined in this manner was $q_O=-1.45$. This result is needed in order to calculate the oddfold crystal-field parameters, which are used in the intensity calculations.

The oddfold crystal-field components were determined from Eq. (4) using $q_O=-1.45$. The odd-k A_{kq} were found to be $A_{32}=849-i827$, $A_{52}=-1715-i105$, $A_{72}=39.1-i10.1$, and $A_{76}=-69.6+i75.5$ cm^{-1}/Å^k. These oddfold A_{kq} were used in conjunction with the B_{kq} of Table V to calculate the Judd-Ofelt parameters, Ω_k, given in Table VI. In the calculation of the Ω_k, the aqueous centroids and the smoothed B_{kq} were used. The Ω_k for Nd^{3+} and Er^{3+} were also calculated using the best-fit B_{kq} and centroids, and as can be seen, the difference is insignificant.

IV. INTENSITY CALCULATIONS

Once the energy levels and wave functions have been computed, the matrix elements for electric dipole and magnetic dipole transitions, for both σ and π polarizations, between each of the levels can be computed. The line strengths, designated by S_{ij}^{ED} and S_{ij}^{MD} for electric and magnetic dipole transitions, respectively, are calcu-

TABLE V. Theoretical crystal-field parameters.

Ion	B_{kq} (cm^{-1}) B_{20}	B_{40}	B_{44}	B_{60}	B_{64}	Im B_{64}
A_{kq} [a]	2758	-1217	1850	-119	419	201
Ce	508	-917	1394	-278	982	472
Pr	484	-787	1196	-223	787	378
Nd	471	-703	1069	-189	667	320
Pm	463	-650	988	-169	596	286
Sm	460	-614	934	-157	554	266
Eu	460	-589	895	-149	524	252
Gd	460	-567	862	-141	498	239
Tb	461	-546	831	-133	471	226
Dy	464	-528	803	-126	445	214
Ho	467	-513	780	-120	424	204
Er	471	-502	763	-117	412	198
Tm	475	-493	750	-115	405	194
Yb	479	-479	729	-108	383	184

[a] $A_{kq}=\frac{1}{2}[A_{kq}^{\text{expt}}(\text{Nd})+A_{q}^{\text{expt}}(\text{Er})]$ in units of $cm^{-1}/Å^{k}$.

lated as described by Leavitt and Morrison.[23]

The radiative lifetime is defined by[24,25]

$$\frac{1}{\tau_{ij}}=\frac{32\pi^3\alpha}{3c^2}\left[\frac{n_{ij}(n_{ij}+2)^2}{9}S_{ij}^{\text{ED}}+n_{ij}^3S_{ij}^{\text{MD}}\right]\nu_{ij}^3 , \quad (5)$$

where α is the fine structure constant and n_{ij} is the index of refraction at the wavelength λ_{ij}.

The index of refraction of NLM was measured by Bakhshieva, Karapetyan, and Morozov[26] using the prism method.[27] They report that instead of the anticipated simple double refraction pattern for an optically uniaxial crystal (two lines corresponding to n_0 and n_e), a superposition of lines is observed, from which they extract a single value for the index of refraction. They report an average value for the index of refraction for five different wavelengths. We have fit their data to the following Sellmeier's dispersion relation:

$$n^2=1+\frac{A\lambda^2}{\lambda^2-B} \quad (6)$$

and obtained $A=2.732\pm0.005$ and $B=0.0262\pm0.0003$ μm^2 in a least-squares fit to the data.

The index of refraction has been reported more recently in the literature by Protasova *et al.*[28] using an immersion method. They also report only a single value for n at each wavelength. A least-squares fit of their data to the same dispersion relation gives $A=2.65\pm0.013$ and $B=0.030\pm0.001$ μm^2.

In making theoretical predictions of radiative lifetimes and other physical parameters from the calculated line-to-line transition probabilities, we need to have the index of refraction as a function of wavelength. We use an index of refraction based on the average of these reported values: $A_{\text{av}}=2.7$ and $B_{\text{av}}=0.028$ μm^2.

The branching ratio as a function of temperature is given by

$$\beta_{ij}=\frac{\frac{Z_i}{\tau_{ij}}}{\sum_{i,j}\frac{Z_i}{\tau_{ij}}} , \quad (7)$$

where the temperature dependence is introduced through the partition function, Z, by assuming the levels of the pumped multiplet are in thermal equilibrium

$$Z_i=\frac{g_i\exp\left[\frac{E_i}{kT}\right]}{\sum_{i'}g_{i'}\exp\left[\frac{E_{i'}}{kT}\right]} . \quad (8)$$

TABLE VI. Calculated Judd-Ofelt intensity parameters Ω_k (10^{-20} cm^2) of rare-earth ions in the La site of $NaLa(MoO_4)_2$ [a]

Ion	Ω_2	Ω_4	Ω_6
Ce	0.357 0	3.161	21.64
Pr	0.199 8	1.596	9.211
Nd	0.192 6	1.013	5.052
Nd [b]	0.192 6	1.014	5.054
Pm	0.111 5	0.785 5	3.885
Sm	0.097 22	0.664 0	3.217
Eu	0.076 91	0.512 4	2.273
Gd	0.060 18	0.391 0	1.567
Tb	0.105 1	0.674 1	3.829
Dy	0.077 30	0.479 4	2.373
Ho	0.063 11	0.381 0	1.731
Er	0.060 51	0.359 2	1.633
Er [b]	0.060 51	0.359 3	1.634
Tm	0.058 86	0.344 5	1.579
Yb	0.049 70	0.282 2	1.202

[a] Smoothed B_{kq} and aqueous centroids.
[b] Best-fit B_{kq} and centroids.

In these equations, i refers to a level in the upper (pumped) multiplet, j refers to a level in the lower multiplet, and g_i is the degeneracy of level i.

V. RESULTS AND DISCUSSION

The computer output containing line-to-line transition probabilities contains an overwhelming amount of information, and it is not practical to include all the results here. We have restricted our analysis to a few multiplets of particular interest. For each pair of multiplets considered, we computed the branching ratios for all possible line-to-line transitions and sorted out the strongest transitions at a given temperature.

For Nd^{3+}, we considered the transitions originating at the $^4F_{3/2}$ level and ending on the four lower multiplets: $^4I_{9/2}$, $^4I_{11/2}$, $^4I_{13/2}$, and $^4I_{15/2}$. We have used Nd^{3+} in some respects as a test case, because Nd^{3+} has been studied extensively in many hosts, and its lasers properties are well known. The multiplet branching ratios are shown schematically in Fig. 3 for Nd^{3+}:NLM from the $^4F_{3/2}$ multiplet.

Stimulated emission of Nd^{3+} is reported by the same groups reporting energy levels in Nd^{3+}:NLM.[7,29] Unlike Nd^{3+}:YAG, the $^4I_{11/2}$ multiplet in NLM is inhomogeneously broadened, and some of the individual Stark components are not well resolved. The fluorescence spectra in Fig. 2 illustrate the qualitative differences in the spectra. There was some discrepancy in the assignment of the Stark levels observed in fluorescence in the $^4I_{11/2}$ manifold, leading to ambiguity in assigning the initial and terminal levels of the fluorescence transitions. Both sets of experimental measurements[7,29] and the theoretical calculations identify the shortest wavelength transition between the $^4F_{3/2}$ and $^4I_{11/2}$ manifolds (level 28 to level 6) at 1.053 μm. All level numbers correspond to the numbering of the levels in Tables III and IV. The most intense fluorescence occurs at longer wavelengths than the

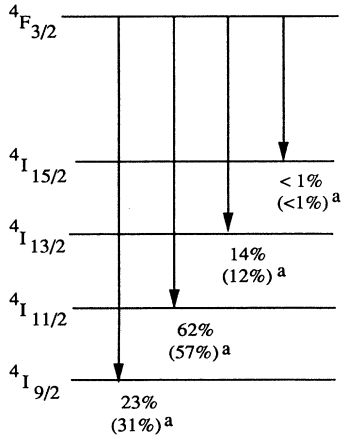

FIG. 3. Multiplet branching ratios for transitions originating at the $^4F_{3/2}$ multiplet of Nd^{3+} in NaLa(MoO$_4$)$_2$. Experimentally measured values are from Harper and Thornton[7] and are indicated by superscript a.

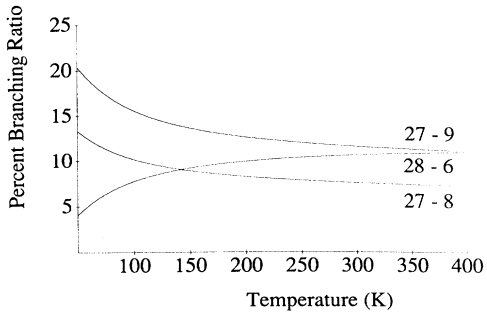

FIG. 4. Line-to-line branching ratios as a function of temperature for transitions originating at the $^4F_{3/2}$ multiplet of Nd^{3+} in NaLa(MoO$_4$)$_2$. The transitions shown are the three strongest transitions at room temperature.

28 to 6 transition. Harper identifies the two strongest transitions in this region at 1.0578 and 1.0658 μm. Morozov *et al.* also identify strong transitions in this region at 1.0597 and 1.0645 μm, but note that the observed relative intensities depend on Nd^{3+} concentration and pump power. Our calculations indicate that the strongest transitions in this region should be 27 to 9 (1.0689 μm) and 27 to 8 (1.0645 μm). The temperature-dependent branching ratios from this analysis are shown in Fig. 4 for the three strongest transitions sorted at room temperature.

For Er^{3+} we have analyzed transitions between the two lowest multiplets ($^4I_{13/2}$ to $^4I_{15/2}$) with wavelengths in the eye-safe spectral region. A plot of the temperature dependence of the strongest transitions is shown in Fig. 5. Two transitions (10 to 4 at 1.595 μm and 10 to 7 at 1.546 μm) increase in strength as the temperature is lowered. The strongest transition at room temperature is 13 to 2 at 1.504 μm. Since level 2 is only 18 cm^{-1} above the ground state, and thus significantly thermally populated at room temperature, this transition is of less interest for laser applications, particularly for cw lasers. As far as we

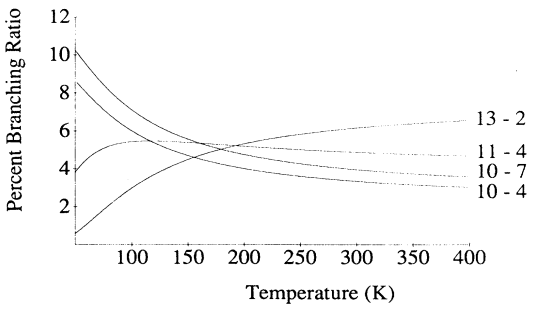

FIG. 5. Line-to-line branching ratios as a function of temperature for transitions originating at the $^4I_{13/2}$ multiplet of Er^{3+} in NaLa(MoO$_4$)$_2$. The transitions shown are the two strongest transitions at room temperature and the two strongest transitions at low temperatures (liquid nitrogen temperature and below).

know, no measurements of stimulated emission of Er^{3+}:NLM have been reported.

The numerical agreement between experimental measurements and theoretical predictions of the multiplet branching ratios is very close. This is consistent with the close agreement of the two sets of Judd-Ofelt parameters for Nd^{3+} and Er^{3+} given in Table VI, based on the two sets of centroids. The results of the multiplet branching ratios are not sensitive to accurate placement of the centroids. The energy difference of two lines is sensitive to the positions of the Stark levels, so the wavelength of the emitted light in the line-to-line calculations is sensitive to the accurate placement of the centroids. However, the qualitative behavior may be predicted accurately based on the crystal-field parameters given in Table V and centroids taken from measured spectra of the ions in aqueous solution. The results of these calculations suggest that the computer techniques outlined in the paper can also be used to predict the behavior of other rare-earth ions in this host material.

ACKNOWLEDGMENTS

This research was sponsored by the Center for Night Vision and Electro-Optics at Ft. Belvoir, VA, where the optical absorption and fluorescence measurements were performed. S.B.S. wishes to thank the National Research Council for financial support.

[1]W. P. Risk and W. Lenth, Opt. Lett. **12**, 993 (1987).

[2]T. H. Allik, W. W. Hovis, D. P. Caffey, and V. King, Opt. Lett. **14**, 116 (1989).

[3]S. R. Bowman, B. J. Feldman, J. M. McMahon, A. P. Bowman, and D. Scarl, in *Tunable Solid State Lasers,* OSA Proceeding Series, edited by M. L. Shand and H. P. Jenssen (Optical Society of America, Washington, D.C., 1989), Vol. 5, pp 108–111.

[4]For recent advances in Er^{3+}, Tm^{3+}, and Ho^{3+} lasers, see *Digest of Topical Meeting on Advanced Solid-State Lasers,* Salt Lake City, Utah, 1990 (Optical Society of America, Washington, D.C., 1990).

[5]J. J. Zayhowski, J. Ochoa, and A. Mooradian, Opt. Lett. **14**, 1318 (1989).

[6]J. J. Zayhowski and A. Mooradian, Opt. Lett. **14**, 24 (1989).

[7]L. L. Harper and J. R. Thornton, Technical Report No. AFALTR-72-38, Air Force Avionics Laboratory, WPAFB, 1972 (unpublished).

[8]G. M. Zverev and G. Ya. Kolodny, Zh. Eksp. Teor. Fiz. **52**, 337 (1967). [Sov. Phys. JETP **25**, 217 (1967)].

[9]A. M. Morozov, M. N. Tolstoi, and P. P. Feofilov, Opt. Spektrosk. **22**, 258 (1967) [Opt. Spectrosc. (USSR) **22**, 139 (1967)].

[10]S. A. Pollack, D. B. Chang, and N. L. Moise, J. Appl. Phys. **60**, 4077 (1986).

[11]V. K. Trunov, A. A. Evdokimov, T. P. Rybakova, and T. A. Berezina, Russ. J. Inorg. Chem. **24**, 93 (1979).

[12]T. Zoltai and J. H. Stout, *Minerology* (Burgess, Minneapolis, 1984), p. 445.

[13]G. M. Sheldrick, SHELXTL User's Manual, Revision 5.1, Nicolet Corporation, Madison, WI, 1986.

[14]*International Tables for X-ray Crystallography,* edited by N. Henry and K. Lonsdale, (Kynoch, Birmingham, England, 1969), Vol. I.

[15]T. H. Allik, S. A. Stewart, D. K. Sardar, G. J. Quarles, R. C. Powell, M. R. Kokta, W. W. Hovis, and A. A. Pinto, Phys. Rev. B **37**, 9129 (1988).

[16]T. H. Allik, C. A. Morrison, J. B. Gruber, and M. R. Kokta, Phys. Rev. B **41**, 21 (1990).

[17]B. G. Wybourne, *Spectroscopic Properties of Rare Earths* (Wiley, New York, 1965).

[18]W. T. Carnall, P. R. Fields, and K. Rajnak, J. Chem. Phys. **49**, 4412 (1968); **49**, 4424 (1968); **49**, 4443 (1968); **49**, 4447 (1968); **49**, 4450 (1968).

[19]C. A. Morrison and R. P. Leavitt, J. Chem. Phys. **71**, 2366 (1979).

[20]C. A. Morrison, *Angular Momentum Theory Applied to Interactions in Solids,* Lecture Notes in Chemistry Vol. 47, (Springer Verlag, New York, 1988).

[21]D. E. Onopko, *Spektroskopiya Tverdogo Tela* (Nauka, Moscow, 1969), Vol. IV, p. 15.

[22]C. A. Morrison and R. P. Leavitt, in *Handbook on the Physics and Chemistry of Rare Earths,* edited by K. A. Gschneidner and L. Eyring (North Holland, New York, 1982), Vol. 5.

[23]R. P. Leavitt and C. A. Morrison, J. Chem. Phys. **73**, 749 (1980).

[24]S. Hufner, *Optical Spectra of Transparent Rare Earth Compounds* (Academic, New York, 1978).

[25]E. D. Filer, C. A. Morrison, N. P. Barnes, and G. T. Turner, in *Advanced Solid State Lasers,* OSA Proceeding Series (Optical Society of America, Washington, D.C., in press).

[26]G. F. Bakhshieva, V. E. Karapetyan, and A. M. Morozov, Opt. Spektrosk. **20**, 918 (1966) [Opt. Spectrosc (USSR) **20**, 510 (1966)].

[27]W. L. Bond, J. Appl. Phys. **36**, 1674 (1965).

[28]V. I. Protasova, B. M. Ayupov, L. Yu. Kharchenko, L. P. Koseeva, and V. F. Nesterenko, Izv. Sib. Otd. Akad. Nauk SSSR, Ser. Khim. Nauk (1), 58 (1989).

[29]A. M. Morozov, M. N. Tolstoi, P. P. Feofilov, and V. N. Shapovalov, Opt. Spektrosk. **22**, 414 (1967) [Opt. Spectrosc. (USSR) **22**, 224 (1967)].